Applied Mathematical Modelling 39 (2015) 500–514

Contents lists available at ScienceDirect

Applied Mathematical Modelling

journal homepage: www.elsevier.com/locate/apm

Multi-objective active control policy design for commensurate and incommensurate fractional order chaotic financial systems

Indranil Pan [a,*], Saptarshi Das [b], Shantanu Das [c]

[a] Energy, Environment, Modelling and Minerals (E^2M^2) Research Section, Department of Earth Science and Engineering, Imperial College London, Exhibition Road, London SW7 2AZ, United Kingdom
[b] Communications, Signal Processing and Control (CSPC) Group, School of Electronics and Computer Science, University of Southampton, Southampton SO17 1BJ, United Kingdom
[c] Reactor Control Division, Bhabha Atomic Research Centre, Mumbai 400085, India

ARTICLE INFO

Article history:
Received 5 January 2013
Received in revised form 29 March 2014
Accepted 3 June 2014
Available online 17 June 2014

Keywords:
Chaos control
Chaotic financial system
Commensurate and incommensurate order system
Fractional order nonlinear systems
Multi-objective active control

ABSTRACT

In this study, an active control policy design is proposed for a fractional order financial system, which considers multiple conflicting objectives. An active control template is used as a nonlinear state feedback mechanism and the controller gains are selected within a multi-objective optimization (MOO) framework to satisfy the conditions of asymptotic stability, which are derived analytically. The MOO obtains a set of solutions on the Pareto optimal front for the multiple conflicting objectives that are considered. We demonstrate that there is a trade-off between the multiple design objectives where better performance for one objective can only be obtained at the cost of degrading the performance for the other objectives. The multi-objective controller design was compared using three different MOO techniques, i.e., non-dominated sorting genetic algorithm-II, epsilon variable multi-objective genetic algorithm, and multi-objective evolutionary algorithm with decomposition. The robustness of the same control policy designed with the nominal system settings was also investigated with gradual decrease in the commensurate and incommensurate fractional orders of the financial system.

1. Introduction

Investigations of the chaotic dynamics of physical systems have identified their presence in various different fields. In particular, financial systems have been shown to exhibit significant chaotic behavior [1]. Fractional calculus-driven modeling techniques, especially fractional Brownian motion, have been a major huge focus as potential tools for describing the dynamical behavior of the stochastic variations in financial time series [2]. Data-driven models of financial systems have been shown to possess power law characteristics, i.e., the Fourier transform spectra decays as a power law with respect to frequency [3,4]. In finance, Meerschaert and Scalas [5] showed that the relationship between random variables such as log-returns and waiting times, are suitable for modeling using fractional order (FO) partial differential equations. FO noise characteristics have also been used to identify periods of economic crisis based on financial time series [6]. The effects of parameter switching on FO chaotic financial systems were studied by Danca et al. [7]. Other perspective on financial

* Corresponding author. Tel.: +44 7448532764.
E-mail addresses: indranil.jj@student.iitd.ac.in, i.pan11@imperial.ac.uk (I. Pan), saptarshi@pe.jusl.ac.in, s.das@soton.ac.uk (S. Das), shantanu@magnum.barc.gov.in (S. Das).

http://dx.doi.org/10.1016/j.apm.2014.06.005
0307-904X/

modeling has also been developed for empirical market data, e.g., the FO volatility model [8]. The concept of FO financial modeling has been extended to variable order financial systems [9] where the FOs change over time. These studies show that sudden large fluctuations in financial time series have power law characteristics and they possess close relationships with fractional calculus. A realistic FO macroeconomic model was estimated using national economic data from the UK, Canada, and Australia by Skovranek et al. [10]. Similarly, nonlinear model parameter estimation has been proposed using least squares to model macroeconomic data from the USA [11] and interest rate changes in Japan [12]. Studies have also shown that the presence of time delays in these financial systems modifies the chaotic behavior of the system where one policy change takes some time to modify the overall system's dynamics [13].

It has been found that complex financial systems exhibit both stochastic and deterministic dynamics, where the first branch has emerged to model typical behaviors such as the non-stationarity, non-Gaussianity, randomness, and long-range dependency (or power law characteristics) of these systems, as discussed earlier. The second branch has emerged to analyze significant nonlinear dynamical behaviors such as chaos, bifurcation [14], and hyper-chaos [15] in large-scale financial systems. Several studies have attempted to investigate chaotic dynamics in financial time series using delay embedding-based phase space reconstruction, Lyapunov exponent estimation based on parametric and nonparametric methods [16], recurrence plots [17], and other approaches. In addition to practical data or time series-based studies, continuous time [14] and discrete time models [18] have been proposed to model the chaotic dynamics of financial systems. Thus, the co-existence of chaotic and FO characteristics is an inherent feature of financial systems, which has motivated the study of active control policies for these systems.

Chaotic dynamics are undesirable and they must be suppressed to reduce financial risks and improve the performance of the economy [17]. Classically, two broad methods are employed for chaos control, i.e., the Ott–Greborgi–Yorke (OGY) method of intermittent control and the continuous control method [19,20]. FO economical or financial systems [21] have been controlled or synchronized using several approaches, e.g., sliding mode [22], time-delayed feedback [23], linear control [24], lag projective synchronization [25], Lyapunov linearization, and stability condition [26]. In [27], the control of an uncertain FO financial system was addressed using an adaptive sliding mode control. However, in all of these examples, chaos control was addressed from a stability viewpoint where the control performance was not considered. Other computational intelligence-based techniques that use intelligent algorithms for chaos control [28], [29] or synchronization [30] include performance measures based on rapid synchronization or control in the formulation of the objective function itself. However, the drawback of this type of design method is that guaranteed analytical stability is not enforced during the process so the scheme might not work with initial conditions other than those used in the simulation. In addition, only single objectives were considered as performance measures in the designs reported in [29,30]. In practical design problems, there are multiple trade-offs among a set of conflicting objectives. Therefore, a design methodology must consider these challenges and obtain optimal solutions that satisfy these objectives adequately. In other words, it is necessary to apply multi-objective optimization (MOO) methods to these problems to obtain efficient designs.

Multi-objective synchronization for chaotic systems has been investigated recently [31], where the coupling strengths between two chaotic systems are optimized using evolutionary MOO. In this case, however, analytical stability is not included within the optimization algorithm. Thus, chaotic systems might not synchronize using the proposed methodology [31] if the values of the initial conditions are different. This is because the synchronization is only achieved in a mean squared sense and the guaranteed analytical stability of the error dynamical system is not enforced. In the present study, we extend the concept of the multi-objective synchronization of chaotic systems [31] to chaos control. In contrast the previously described approach [31], we incorporate the analytical stability conditions for chaos control within the optimization algorithm itself. This ensures the stability of the optimized solutions in all cases, even when considering different initial conditions. To the best of our knowledge, the present study is the first active control policy design for commensurate and incommensurate FO chaotic systems in a multi-objective framework with guaranteed analytical stability considerations.

The remainder of this paper is organized as follows. Section 2 outlines the preliminary background of the fractional calculus and the numerical methods for simulating FO chaotic systems. Section 3 introduces the FO financial system and proposes the mathematical underpinnings of the active control strategy. Section 4 highlights the need for MOO in chaos control and provides brief descriptions of the non-dominated sorting genetic algorithm-II (NSGA-II), epsilon variable multi-objective genetic algorithm (εv-MOGA), and multi-objective evolutionary algorithm with decomposition (MOEA/D) as multi-objective optimizers. Section 5 presents the results and discussions. Section 6 gives our conclusions.

2. Mathematical preliminaries

2.1. Basics of fractional calculus

Fractional calculus is an extension of integer order successive differentiation and integration for any arbitrary real order. The fundamental operator that represents non-integer order differentiation or integration is given by ${}_aD_t^{\alpha}$ in (1), where $\alpha \in \mathbb{R}$ is the order of the differ-integration and a and t are the bounds of the operation.

$$ {}_aD_t^{\alpha} = \begin{cases} d^{\alpha}/dt^{\alpha}, & \alpha > 0, \\ 1, & \alpha = 0, \\ \int_a^t (d\tau)^{\alpha}, & \alpha < 0. \end{cases} \tag{1} $$

There are three main definitions of fractional calculus, i.e., Grünwald–Letnikov, Riemann–Liouville, and Caputo. There are also other definitions such as those of Weyl, Fourier, Cauchy, Abel, and Nishimoto. In FO systems and control-related studies, Caputo's fractional differentiation formula is generally preferred. This typical definition of a fractional derivative is generally used to derive FO transfer function models from FO ordinary differential equations with zero initial conditions. According to Caputo's definition, the αth order derivative of a function $f(t)$ with respect to time is given by (2)

$$ {}_aD_t^{\alpha} f(t) = \frac{1}{\Gamma(m-\alpha)} \int_a^t \frac{D^m f(t)}{(t-\tau)^{\alpha+1-m}} d\tau, \quad \alpha \in \mathbb{R}^+, \quad m \in \mathbb{Z}^+, \quad m-1 \le \alpha < m, \tag{2} $$

where, $\Gamma(\alpha) = \int_0^t e^{-t} t^{\alpha-1} dt$ is Euler's Gamma function. We use this definition to implement the fractional integro-differential operators of the chaotic system. The Caputo definition of a fractional derivative is advantageous for control-related applications compared with the Riemann–Liouville definition because it only requires the initial conditions for integer order derivatives and not the initial conditions of the fractional derivatives. The Laplace transform of the Caputo fractional derivative is given by (3) [32].

$$ \mathcal{L}\left[{}_0D_t^{\alpha} f(t)\right] = \int_0^{\infty} e^{-st} {}_0D_t^{\alpha} f(t) dt = s^{\alpha} F(s) - \sum_{k=0}^{m-1} s^{\alpha-k-1} f^m(0), \quad m-1 \leqslant \alpha < m. \tag{3} $$

For zero initial conditions, the Laplace transform of the three definitions amounts to the same expression $s^{\alpha}F(s)$, which is used extensively in many modern control applications. In addition, continuous or discrete time rational approximation techniques for the FO differ-integrator $s^{\pm\alpha}$ are often employed in simulations [33].

2.2. Numerical method for simulating FO chaotic systems

Chaotic coupled differential equations can be simulated numerically using the power series expansion method, Adams–Bashford–Moulton predictor corrector method [34], continued fraction expansion (CFE) method [35], and other approaches. As shown by Petras [32], the chaotic FO differential equations in (4) can be written in the form of a set of integral equations, as in (7), and band-limited rational approximations can be used for the fractional differentials. This method is used in the present study to simulate the FO chaotic system.

For a set of coupled fractional differential equations of the form (4),

$$ \begin{aligned} {}_0D_t^{q1} x(t) &= f(x(t), y(t), z(t)), \\ {}_0D_t^{q2} y(t) &= g(x(t), y(t), z(t)), \\ {}_0D_t^{q3} z(t) &= h(x(t), y(t), z(t)), \end{aligned} \tag{4} $$

considering that the fractional differ-integrals are linear operators, i.e.,

$$ {}_aD_t^{\alpha}(\lambda f(t) + \mu g(t)) = \lambda {}_aD_t^{\alpha} f(t) + \mu {}_aD_t^{\alpha} g(t), \tag{5} $$

and that the FO derivative commutes with the integer order derivative, i.e.,

$$ \frac{d^n}{dt^n}\left({}_aD_t^{\alpha} f(t)\right) = {}_aD_t^{\alpha}\left(\frac{d^n f(t)}{dt^n}\right) = {}_aD_t^{\alpha+n} f(t). \tag{6} $$

Eq. (4) can also be written in the form of integral equations as (7).

$$ \begin{aligned} x(t) &= {}_0D_t^{1-q_1}\left(\int_0^t [f(x(t), y(t), z(t))] dt\right), \\ y(t) &= {}_0D_t^{1-q_2}\left(\int_0^t [g(x(t), y(t), z(t))] dt\right), \\ z(t) &= {}_0D_t^{1-q_3}\left(\int_0^t [h(x(t), y(t), z(t))] dt\right). \end{aligned} \tag{7} $$

An implementation of this transformation in a Matlab/Simulink based environment is capable of simulating FO chaotic systems, as shown by Petras [32].

Each value of the FO differ-integrals $\{1-q_1, 1-q_2, 1-q_3\}$ is rationalized with Oustaloup's 5th order rational approximation [36]. The FO differ-integrals are basically infinite dimensional linear filters. However, band-limited realizations of FO elements are necessary for simulations. In the present simulation study, each FO element is rationalized with Oustaloup's recursive filter [36], which is given by Eqs. (8) and (9). If it is assumed that the expected fitting range or frequency range of the controller operation is (ω_b, ω_h), then the higher order filter that approximates the FO element s^{α} can be written as (8) [37]:

$$G_f(s) = s^{\alpha} = K\prod_{k=-N}^{N}\frac{s+\omega'_k}{s+\omega_k}, \tag{8}$$

where the poles, zeros, and gain of the filter can be evaluated as follows

$$\omega_k = \omega_b(\omega_h/\omega_b)^{\frac{k+N+\frac{1}{2}(1+\alpha)}{2N+1}}, \quad \omega'_k = \omega_b(\omega_h/\omega_b)^{\frac{k+N+\frac{1}{2}(1-\alpha)}{2N+1}}, \quad K = \omega_h^{\alpha}. \tag{9}$$

In Eqs. (8) and (9), α is the order of the differ-integration and $(2N+1)$ is the order of the filter. In the present study, we apply a 5th order Oustaloup rational approximation to the FO elements within the frequency range $\omega \in \{10^{-2}, 10^{2}\}$ rad/s [36,37].

3. System description and theoretical formulation

The FO chaotic financial dynamical system [21] is given by (10).

$$\begin{aligned}\frac{d^{q_1}x}{dt} &= z + (y-a)x,\\ \frac{d^{q_2}y}{dt} &= 1 - by - x^2,\\ \frac{d^{q_3}z}{dt} &= -x - cz.\end{aligned} \tag{10}$$

The state variables x, y, z represent respectively the interest rate, the investment demand, and the price index of a financial system, respectively. The first state variable (x), which is the interest rate, can be influenced by the surplus between investment and savings as well as structural adjustments of the prices. The second state variable (y) is in proportion to the rate of investment, and inversely proportional to the cost of investment and the interest rate. The third state variable (z) depends on the difference between supply and demand in the market, and it is also influenced by the inflation rate [14]. The three constant coefficients $\{a, b, c\}$ represent the savings amount, the cost per investment, and the elasticity of the demand of commercial markets, respectively. Figs. 1 and 2 show the variation in the three state variables, i.e., the interest rate, investment demand, and price index, with time (in days) [10] for the commensurate and incommensurate FO financial systems, respectively. All three time series exhibit erratic fluctuations for both systems, thereby leading to chaotic motion in the respective phase space diagrams. The second state variable (investment demand) exhibits more rapid fluctuations than the other two states, thereby indicating the high spectral power in the high frequency operation. Further details of the fractional financial system and its control are reported in Pan et al. [29]. Although stochastic modeling of financial systems has been reported previously, the chaotic deterministic model of financial systems is more popular for the development of effective control policies.

For the active control of the system described by (10), three active control functions $u_1(t)$, $u_2(t)$, $u_3(t)$ can be applied to each of the three states of the system in (10) to yield the following set of equations.

$$\begin{aligned}\frac{d^{q_1}x}{dt} &= z + (y-a)x + u_1(t),\\ \frac{d^{q_2}y}{dt} &= 1 - by - x^2 + u_2(t),\\ \frac{d^{q_3}z}{dt} &= -x - cz + u_3(t).\end{aligned} \tag{11}$$

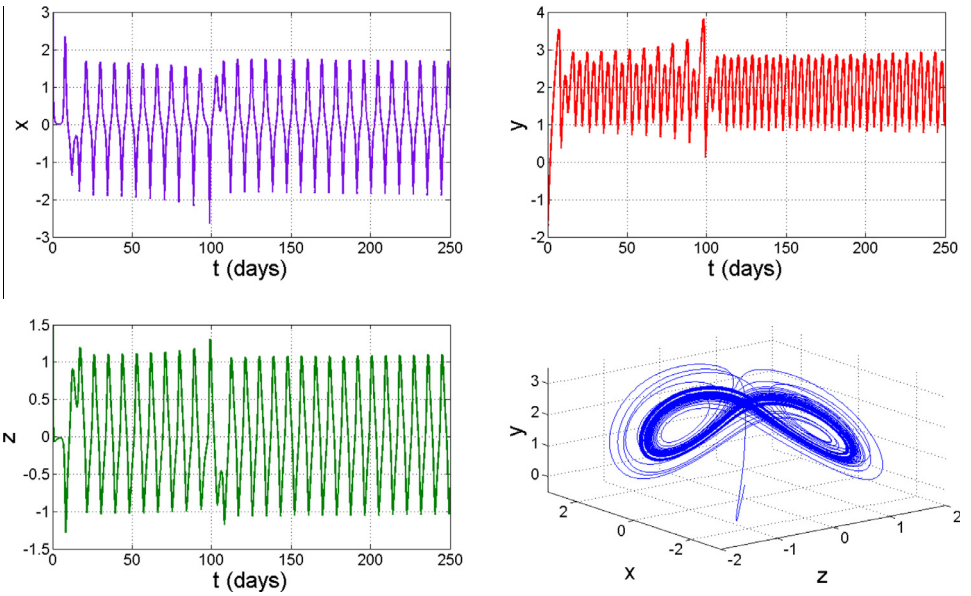

Fig. 1. Phase portrait and state trajectories of the commensurate ($q_1 = q_2 = q_3 = q = 0.9$) FO financial system.

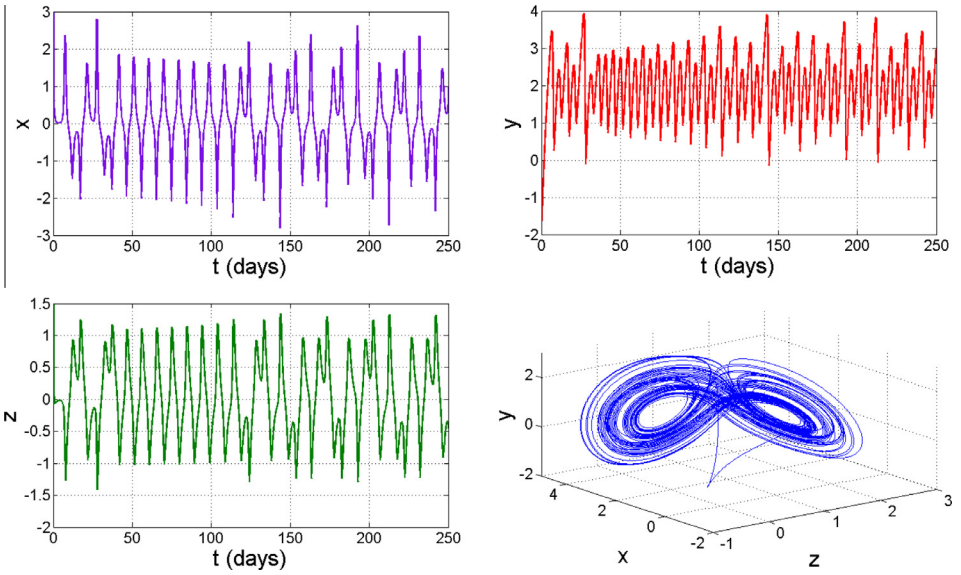

Fig. 2. Phase portrait and state trajectories of the incommensurate ($q_1 = 0.9$, $q_2 = 0.95$, $q_3 = 0.8$) FO financial system.

The nonlinear active state-feedback control functions are selected as (12)–(14) to make the closed loop control system linear.

$$u_1(t) = V_1(t) - xy, \tag{12}$$

$$u_2(t) = V_2(t) - 1 + x^2, \tag{13}$$

$$u_3(t) = V_3(t). \tag{14}$$

The terms $V_i(t) \forall\, i \in \{1, 2, 3\}$ are linear functions of the three system state variables $\{x, y, z\}$. Using Eqs. (12)–(14) in Eq. (11), we obtain (15).

$$\begin{aligned} \tfrac{d^{q_1}x}{dt} &= z - ax + V_1(t), \\ \tfrac{d^{q_2}y}{dt} &= -by + V_2(t), \\ \tfrac{d^{q_3}z}{dt} &= -x - cz + V_3(t). \end{aligned} \tag{15}$$

The active control terms $V_i(t) \forall\, i \in \{1, 2, 3\}$ can be represented by (16), where the constants $m_{ij} \in \mathbb{R},\ \forall i, j \in \{1, 2, 3\}$.

$$\begin{bmatrix} V_1 \\ V_2 \\ V_3 \end{bmatrix} = \begin{bmatrix} m_{11} & m_{12} & m_{13} \\ m_{21} & m_{22} & m_{23} \\ m_{31} & m_{32} & m_{33} \end{bmatrix} \begin{bmatrix} x \\ y \\ z \end{bmatrix}. \tag{16}$$

Thus, (15) and (16) can be combined to obtain (17):

$$D^q \begin{bmatrix} x \\ y \\ z \end{bmatrix} = P \begin{bmatrix} x \\ y \\ z \end{bmatrix} = \begin{bmatrix} -a + m_{11} & m_{12} & 1 + m_{13} \\ m_{21} & -b + m_{22} & m_{23} \\ -1 + m_{31} & m_{32} & -c + m_{33} \end{bmatrix} \begin{bmatrix} x \\ y \\ z \end{bmatrix}, \tag{17}$$

where $q = [q_1, q_2, q_3]^T \in (0, 2)$.

The presence of the squared and cross-product terms of the state variables in the active control inputs in (12)–(14) can be viewed as a nonlinear state feedback control design for commensurate and incommensurate FO systems. The nonlinear control inputs linearize the closed loop system to facilitate the establishment of analytical stabilization schemes [32] for commensurate and incommensurate FO linear systems because the analytical stability design for the nonlinear counterpart is more involved and difficult to design.

The elements of the matrix in (16) are real. Hence, it may be diagonalized to produce an equivalent control action where each of the control signals is a function of its own state only and not the other states. This would remove the number of couplings and reduce the complications in the design process. The number of elements that need to be selected is three instead of nine, which would reduce the burden on the optimization algorithm. However, in many cases, the eigenvalues obtained by the diagonalization might be complex conjugates, thus the physical realization of state-feedback controllers with complex gains would be infeasible. Therefore, all nine components are selected using the optimization in (16) instead of selecting

the diagonals only in our proposed approach. Another aspect of the control action that can be deduced from Eqs. (12)–(14) is that when the individual states become zero due to the application of the control action, i.e., $x = y = z = 0$, then u_2 becomes (-1) and, u_1 and u_3 become zero.

Next, to ensure the asymptotic stability of system (17), the constants m_{ij} must be selected such that the eigenvalues (λ_k) of matrix P satisfy the following condition, which known as Matignon's theorem [38]:

$$|\arg(eig(P))| = |\arg(\lambda_k)| > \frac{q\pi}{2}, \quad 0 < q < 2, \tag{18}$$

for the commensurate FO system where $q_1 = q_2 = q_3 = q$.

For the incommensurate FO system, the asymptotic stability of Eq. (17) can be derived using Deng's theorem as outlined in [39]. Let the incommensurate orders q_i of Eq. (17) be written in the form $q_i = v_i/u_i, u_i, v_i \in \mathbb{Z}_+$. Let m be the lowest common multiple (LCM) of u_i and let $\gamma = 1/m$.

The characteristic equation can then be derived from (17) as shown in (19) by denoting the FO operators s^{q_i} by λ^{mq_i}, where *diag* denotes a diagonal matrix [39,40].

$$\det(s^{q_i}I - P) = \det\left(diag\left[\begin{array}{ccc}\lambda^{mq_1} & \lambda^{mq_2} & \lambda^{mq_3}\end{array}\right] - P\right) = \det\begin{bmatrix}\lambda^{mq_1} + a - m_{11} & -m_{12} & -1 - m_{13} \\ -m_{21} & \lambda^{mq_2} + b - m_{22} & -m_{23} \\ 1 - m_{31} & -m_{32} & \lambda^{mq_3} + c - m_{33}\end{bmatrix} = 0. \tag{19}$$

If all the roots $\lambda_i,\ \forall i \in [1,2,3]$ of the characteristic equation, as given in Eq. (19), satisfy $|\arg(\lambda_i)| > \frac{\gamma\pi}{2},\ \forall i \in [1,2,3]$, then the system described by Eq. (17) is stable. The characteristic equation (19) is transformed into a higher integer-order polynomial equation if the incommensurate orders q_i are considered as rational numbers. Matlab's Symbolic Math Toolbox function *solve()* was used in the present study to obtain the roots of the characteristic polynomial equation (19). In this case, m is 20 for the incommensurate orders $q_1 = 0.9$, $q_2 = 0.95$, $q_3 = 0.8$. To check the stability of incommensurate FO systems, it is sufficient to verify the argument of the roots in the primary Riemann sheet only since the hyper-damped and ultra-damped roots in the higher Riemann sheets are always stable. Depending on the rational number representation of the incommensurate orders and by taking their LCM, the number of Riemann sheets can be extremely high and different roots might also be distributed in different higher Riemann sheets but this does not affect the stability of the incommensurate FO system. Therefore, most previous studies only considered the first Riemann sheet for stability checking, as $(\pi/2m) \leqslant |\arg(\lambda_k)| \leqslant (\pi/m)$. Of course, we could place the root at specific locations, even in the higher Riemann sheets, e.g., the placement of ultra-damped roots for commensurate order systems as reported by Bhalekar and Gejji [41]. During optimization-based controller design for both the commensurate and incommensurate FO systems, a constraint is imposed such that at least two roots lie in the stable region of the primary Riemann sheet i.e., $(\pi/2m) \leqslant |\arg(\lambda_k)| \leqslant (\pi/m)$. This allows the design of a relatively fast control system, as opposed to the safe but very slow control operation when all the closed loop poles were pushed to the higher Riemann sheet (i.e., hyper-damped and ultra-damped roots) in the study reported by Das et al. [42].

4. MOO for active control

4.1. Requirements for MOO

In any practical real-world problem with constraints on resources, it is usual that the satisfaction of one criterion to a greater extent will result in the satisfaction of other conflicting criteria to a lesser extent. The concept of Pareto optimality [43] applies this concept to economics in the areas of income distribution and economic efficiency. Given that a finite number of goods are allocated among a set of individuals, if the economic allocation is Pareto efficient, no individual will become better off without one or more individuals being worse off. This same concept can be applied to the controller design problem for financial systems. Thus, there is a trade-off in any controller design problem, as discussed previously [44,45]. The two conflicting objective functions can be selected as the integral of the time multiplied squared error (ITSE) (J_1) and the integral of the squared deviation of controller output (ISDCO) (J_2). These two contradictory objectives can be expressed mathematically as:

$$J_1 = ITSE_{set-point} = \int_{\psi}^{\infty} te_{sp}^2(t)dt, \tag{20}$$

$$J_2 = ISDCO = \int_{\psi}^{\infty} (u(t) - u_{ss})^2 dt, \tag{21}$$

where ψ represents the instant of time when the control signal was applied and e_{sp} represents the error signal, i.e., the deviation of the chaotic trajectory from the desired set-point.

The first objective function J_1 tries to ensure the rapid tracking of the desired set-point. The time multiplication term assigns heavy penalties to errors that occur at later stages, which ensures a faster settling time. The second objective function J_2 tries to reduce the change in the control signal because large control signal deviations necessitate large changes in the manipulated variables, which are not desirable [46]. This is because the manipulated variables are physical quantities and this might result in shocks to the system. J_2 is given by Eq. (21) and the term $\Delta u(t) = u(t) - u_{ss}$ represents the change in

the absolute value of the control signal from its steady state value. J_1 and J_2 are conflicting objectives because the controller must exert greater effort to reduce the steady state tracking error or to obtain fast tracking (i.e., to minimize J_1), hence the value of J_2 will increase and vice versa. To evaluate Eqs. (20) and (21), any of the three states x, y, z may be considered, or all of together. The choice depends on the practical constraints of the design. In the present study, we make a trade-off between different conflicting performance objectives by considering only one of the states y to evaluate Eqs. (20) and (21). Therefore, extensive simulations of all possible cases are not reported.

In control design-related optimization problems, there are often conflicts between two or more objectives, i.e., the speed of response and the control effort required [45]. However, this is not obvious for any chosen control objective. For example, several tracking performance measures, such as the integral of the time multiplied absolute error, ITSE, integral of absolute error, and integral of squared error, may yield a Pareto front under a MOO framework but this does not guarantee that these objective are in conflict. The trade-off design is only important when there are physical constraints on arbitrarily increasing one objective while maintaining the other objectives at the same level. Herreros et al. [44] formulated several conflicting objectives in the frequency domain design of linear control systems. However, frequency domain measures cannot be derived for all possible nonlinear chaotic systems. Therefore, in the present study, we rely on the time domain conflict measures, ITSE and ISDCO [45]. This trade-off consideration is also relevant from the viewpoint of financial systems. The three state variables x, y and z represent financial quantities that can be regulated, but which cannot be arbitrarily increased or decreased in a practical setting. Depending on the how the objective functions are framed, we might want to suppress the chaotic oscillations as rapidly as possible while still maintaining the deviations in these state variables and minimizing the control effort required. This might be contradictory so a multi-objective methodology is required in the present scenario.

4.2. NSGA-II algorithm employed for multi-objective controller design

A generalized multi-objective optimization framework can be defined as follows:
Minimize

$$F(x) = (f_1(x), f_2(x), \ldots, f_m(x)), \tag{22}$$

such that $x \in \Omega$, where Ω is the decision space, $\mathbb{R}^m$ is the objective space, and $F : \Omega \to \mathbb{R}^m$ comprises m real valued objective functions.

Let $u = \{u_1, \ldots, u_m\}$, $v = \{v_1, \ldots, v_m\} \in \mathbb{R}^m$ be two vectors and u is said to dominate v if $u_i < v_i \, \forall \, i \in \{1, 2, \ldots, m\}$ and $u \neq v$. A point $x^* \in \Omega$ is called Pareto optimal if $\nexists x | x \in \Omega$ such that $F(x)$ dominates $F(x^*)$. The set of all Pareto optimal points denoted by PS is called the Pareto set. The set of all Pareto objective vectors, $PF = \{F(x) \in \mathbb{R}^m, \; x \in PS\}$, is called the Pareto front. This implies that no other feasible objective vector exists that can improve one objective function without simultaneous degrading some other objective function.

MOEAs that use non-dominated sorting and sharing have higher computational complexity, where they employ a non-elitist approach that requires the specification of a sharing parameter. However, the NSGA-II eliminates these problems and it can find a better spread of solutions with better convergence close to the actual Pareto optimal front [47]. The pseudo-code for the NSGA-II is as follows [47,48].

```
NSGA II Algorithm
Step 1: generate population P_0 randomly
Step 2: set P_0 = (F_1, F_2, ...) = non-dominated-sort (P_0)
Step 3: for all F_i ∈ P_0
  crowding-distance-assignment (F_i)
Step 4: set t = 0
  while (not completed)
    generate child population Q_t from P_t
    set R_t = P_t ∪ Q_t
    set F = (F_1, F_2, ...) = non-dominated-sort (R_t)
    set P_{t+1} = φ
    i = 1
    while |P_{t+1}| + |F_i| < N
      crowding-distance-assignment (F_i)
      P_{t+1} = P_{t+1} ∪ F_i
      i = i + 1
    end
    sort F_i on crowding distances
    set P_{t+1} = P_{t+1} ∪ F_i [1 : (N − |P_{t+1}|)]
    set t = t + 1
  end
return F_1
```

In this case, N represents the number of chromosomes in the population, i.e., the population size. The NSGA-II converts M different objectives into one fitness measure by composing distinct fronts, which are sorted based on the principle of non-domination. During the process of fitness assignment, the solution set that is not dominated by any other solutions in the population is designated as the first front F_1 and these solutions are given the highest fitness value. These solutions are then excluded and the second non-dominated front is created from the remaining population F_2 and ascribed the second highest fitness. This method is iterated until all the solutions are assigned a fitness value. The crowding distance is the normalized distance between a solution vector and its closest neighboring solution vectors in each of the fronts. All of the constituent elements of the front are assigned crowding distances, which are used later for niching. The selection is determined in tournaments of size 2 according to the following logics.

(a) If the solution vector lies on a lower front than its opponent, then it is selected.
(b) If both the solution vectors are on the same front, then the solution with the highest crowding distance wins. This approach retains the solution vectors in the regions of the front that are scarcely populated.

The population size is taken as 100 and the algorithm is run until the cumulative change in fitness function value is less than the function tolerance of 10^{-4} over 100 generations. The crossover fraction is taken as 0.8 and an intermediate crossover scheme is adopted. The mutation fraction is taken as 0.2. To select the parent vectors based on their scaled fitness values, the algorithm uses a tournament selection method with a tournament size of 2. The Pareto front population fraction is taken as 0.7. This parameter indicates the fraction of the population that the solver tests to limit the Pareto front. The optimization variables are the components of the active control functions, i.e., $m_{ij}\,\forall\, i,j \in \{1,2,3\}$. Thus, there are nine optimization variables in total. To ensure that the solutions obtained are guaranteed to be stable, the stability criteria given by Matignon's theorem for commensurate and incommensurate FO system are incorporated into the algorithm during each objective function evaluation. Thus, the solutions that are generated by cross-over, mutation, or reproduction in each generation are tested first to determine whether they satisfy the stability criteria. If the criteria are satisfied, the objective function is evaluated by simulating the chaotic system with the optimum controller gains obtained using the NSGA-II algorithm. If the criteria are not satisfied, then a high value objective function is assigned to the solution without simulating the chaotic system because that particular controller cannot stabilize the system. This automatically assigns a fitness that is worse than the others to these unstable solutions. Therefore, over the generations, the algorithm rejects the unstable solutions and converges toward those regions in the solution space that give stable controller values.

4.3. Testing two other MOO algorithms for the controller design: εv-MOGA and MOEA/D

To facilitate comparisons with the results obtained using the NSGA-II algorithm, two other popular MOO algorithms are also used for active control policy design, i.e., εv-MOGA and MOEA/D. The ε-MOGA is an elitist multi-objective evolutionary algorithm based on the concept of ε-dominance, as discussed in Laumanns et al. [49]. In Deb et al. [50], a comparison of ε-MOEA was performed with other algorithms, such as NSGA-II, Pareto envelope-based selection algorithm, and strength Pareto evolutionary algorithm-II, where εv-MOGA was found to be superior. The ε-MOGA variable (εv-MOGA) is an improved version of εv-MOGA, which can characterize the Pareto front better than the ε-MOGA algorithm with several test-bench functions, as reported by Martínez-Iranzo et al. [51]. The εv-MOGA generates an ε-Pareto set (Θ_p^*), which aims to converge on the actual Pareto optimal set by adjusting the anchor points of the Pareto front $J(\Theta_p^*)$ dynamically while preventing the ends of the Pareto front from being eliminated over the generations [52]. To achieve this, the objective space is divided into a fixed number of boxes, n_box_i, which are specified by the user when the algorithm starts. The algorithm comprises a main population of size N_{ind_P}, an auxiliary population of size N_{ind_G}, and an archive that stores the intermediate solutions, which has an upper limit of $N_{ind\_max\_A}$ = 300. The maximum number of generations is t_{max} = 2500. In the present simulation, N_{ind_G} is 10, N_{ind_P} is 30, $n\_box = [1000 \quad 1000]$, the lower bounds of the variables are $\theta_{li} = [-5 \quad -5 \quad -5 \quad -5 \quad -5 \quad -5 \quad -5 \quad -5 \quad -5 \quad -5]$, and the upper bounds of the variables are $\theta_{ui} = [5 \quad 5 \quad 5 \quad 5 \quad 5 \quad 5 \quad 5 \quad 5 \quad 5 \quad 5]$.

The MOEA/D algorithm proposed by Zhang and Li [53] decomposes the MOO problem into a number of scalar optimization sub-problems and it optimizes them simultaneously. The MOEA/D performs better than the NSGA-II algorithm on test bench problems and it also has a lower computational complexity than the NSGA-II [53]. In the present study, the population size is 70, the number of iterations is 1000, and the Tchebycheff approach is used for decomposition. The Tchebycheff approach associates a weight vector to each of the scalar sub-problems and different Pareto optimal solutions can be obtained by changing modifying its value. One of the pit falls of this approach, is that its aggregation function is not smooth, but it can be used in the MOEA framework because there is no need to calculate the derivative of the aggregation function [53].

5. Simulations and results

5.1. Control of commensurate FO financial systems

The system in (17) is simulated with the commensurate order $q_1 = q_2 = q_3 = q = 0.9$. The initial states $\{x_0, y_0, z_0\}$ of the system are set as $\{2, -1, 1\}$. Fig. 3 shows the Pareto optimal set of solutions obtained using the NSGA-II algorithm. Each of the points represents a particular selection of the active control functions in (16) using three different MOO algorithms. The two

axes denote the conflicting objectives of rapid synchronization performance and lower controller effort. It can be seen that each of these solutions satisfies the objectives to different extents. These solutions are non-dominated in the sense that it is not possible to find another set of solutions that would result in performance improvements for both objectives. Thus, there is a trade-off and a solution that obtains a better performance in terms of one of the objectives would result in a lower performance in terms of the other objective. The stability condition given in (18) is checked as a sub-problem inside the MOO algorithms, thus these Pareto solutions are asymptotically stable. All of the simulations reported in the present study are based on a finite time window of $T = 50$ s.

Table 1 shows set of representative solutions from the Pareto front. These solutions are the solutions at the extreme end of the Pareto front and the median solution. Table 1 shows the numerical values of the coefficients of the active control function in (16) as well as the values of the two conflicting objectives given in (20) and (21). To verify that the three solutions selected (for both the commensurate and incommensurate order systems) are indeed obtained by satisfying Matignon's stability criterion, Table 2 shows that the arguments of the controlled system roots (at least two principal roots) lie in the stable region of the primary Riemann sheet [33].

Fig. 4 shows the time domain evolution of the states of the chaotic system and the control input in the second state u_2. In all cases, the time domain performance of the second state and the controller effort required in the second state are considered in the objective functions of Eqs. (20) and (21), similar to that in [29]. Fig. 4 shows that the y-state variable settles to the equilibrium point very rapidly in solution A_1 followed by solution B_1 whereas solution C_1 is the slowest and it takes a long time to reach equilibrium. In a practical setting, it is always desirable that the chaos is controlled within the shortest possible time. Thus, considering the time domain performance objective, solution A_1 is the best and solution C_1 is the worst. However, the opposite is true in terms of the controller effort. It can be seen that solution A_1 requires a control signal with a larger magnitude than solutions B_1 or C_1. In a real world case, the manipulated variable or the controller effort should be as small as possible because large changes in the manipulated variable might result in physical shocks to the system, or they might not be possible to implement due to other constraints. Therefore, solution C_1 is the best when considering the objective of a lower control signal and solution A_1 is the worst.

It is known that chaotic behavior is observed in the FO financial system for specific values of the coefficients and orders of the state variables (q_1, q_2, q_3), as reported by Chen et al. [21]. We consider these specific values as the nominal financial system during active nonlinear state feedback controller design because it exhibits chaos with the suggested parameters reported in [21]. However, to show that the proposed design technique works reliably with other FOs using the same system structure and the same coefficients, we decrease the commensurate and incommensurate orders gradually. Our results show that as the FO decreases gradually, the chaotic behavior disappears with $q = 0.8$ in the commensurate FO financial system. Fig. 5 shows that the same controller parameters (median solution on the Pareto front) can also suppress chaotic oscillations for other values of the commensurate FOs. They also satisfy the analytical stability conditions in this case. However, the controller parameters might not always be as robust for other systems because the issue of robustness is not considered explicitly in the analytical formulation of the controller design. To design robust controllers, the same multi-objective methodology can be applied, but the mathematical stability formulation must be changed in an appropriate manner.

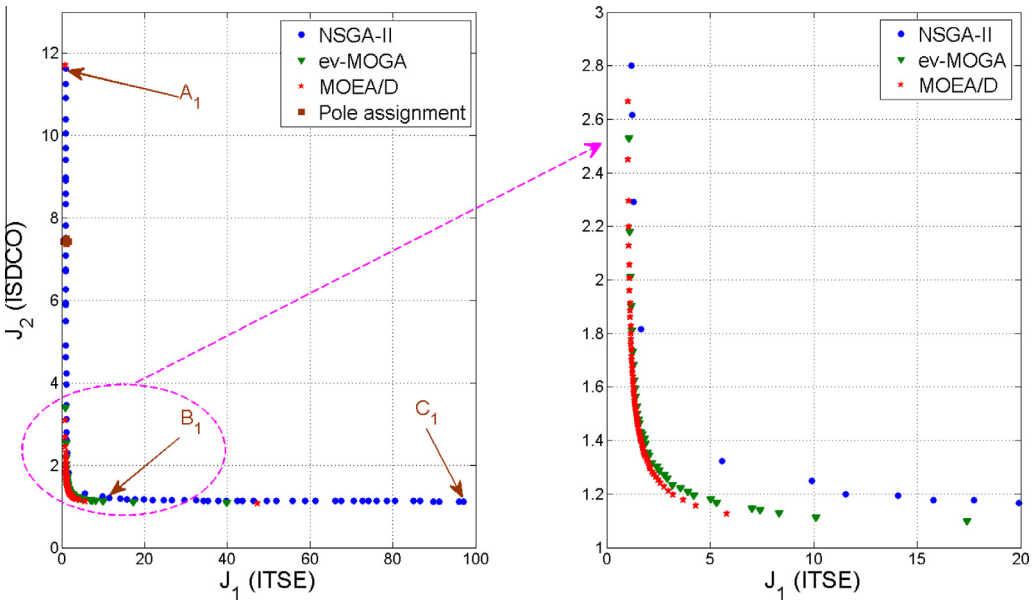

Fig. 3. Pareto optimal front for commensurate FO financial system.

Table 1
Representative solutions on the Pareto front for the commensurate and incommensurate FO financial system.

Class of FO model	Solution points	J_1	J_2	m_{11}	m_{12}	m_{13}	m_{21}	m_{22}	m_{23}	m_{31}	m_{32}	m_{33}
Commensurate	A_1	1.005	11.627	2.300	0.607	1.633	1.357	−2.133	1.041	−0.663	0.818	−0.129
	B_1	9.921	1.248	2.049	0.902	0.708	−2.412	−0.747	0.000	0.572	−0.033	0.757
	C_1	97.152	1.125	2.044	0.948	0.583	−2.449	−0.543	−0.049	0.649	−0.038	0.897
Incommensurate	A_2	1.001	15.995	4.999	−0.018	3.312	3.259	−4.880	0.357	0.959	4.934	−0.920
	B_2	2.224	1.477	3.124	0.188	2.251	−0.625	−0.445	−1.673	−0.517	0.214	−1.250
	C_2	38.298	1.053	2.975	0.485	1.838	−1.089	−0.255	−1.925	−1.803	−0.413	−1.385

Table 2
Guaranteed stability for the three solutions on the Pareto front for two classes of FO financial systems.

Class of FO model	Stability region (in degrees)	Solution points	Argument of the eigenvalues of matrix P (in degrees) lying in the primary Riemann sheet	
Commensurate order $q = 0.85$	$q\pi/2 = 81$	A_1	81.0756	−81.0756
		B_1	83.289	−83.289
		C_1	81.1305	−81.1305
Incommensurate orders $q_1 = 0.9$, $q_2 = 0.95$, $q_3 = 0.8$	$\pi/2m = 4.5$	A_2	−8.3496	8.3496
		B_2	−7.1514	7.1514
		C_2	6.1084	−6.1084

5.2. Control of incommensurate FO financial systems

We simulate the system in (17) with the incommensurate order $q_1 = 0.9$, $q_2 = 0.95$, $q_3 = 0.8$. The initial states $\{x_0, y_0, z_0\}$ of the system are set as $\{2, -1, 1\}$. Fig. 6 shows the Pareto optimal solutions for the incommensurate order case. The difference between this simulation and the previous one is that a different stability condition is checked as a sub-problem in the MOO algorithms, as discussed previously. Three representative solutions on the Pareto fronts (those at the extreme ends and the median solution) are shown in Table 1 and their corresponding time domain performances are shown in Fig. 7. Of the two Pareto fronts in Figs. 6 and 3, it can be seen that the extent of the Pareto front is greater for the incommensurate order example. This implies that when the FOs of the chaotic system are different, more variations are possible in the controller design and the trade-offs that can be achieved among the different performance indices are greater.

For both the commensurate and incommensurate FO financial systems, the Pareto fronts obtained using the three MOO algorithms, i.e., NSGA-II, εv-MOGA, and MOEA/D, are shown in Figs. 3 and 6, respectively. These simulations show that the MOEA/D solutions are better compared with those obtained using εv-MOGA and NSGA-II (indicating that they are much fitter), but the total spread of the Pareto front is much smaller using εv-MOGA and MOEA/D. Therefore, to obtain a wide range of solutions for successful trade-off design, we should consider the results with a larger Pareto front. In the present study, we determined the time domain solutions of the worst, best, and median solutions of the Pareto front with respect to either of the two control objectives. Similar studies could be possible if the financial control policy designer gives a higher priority to non-domination rather than the length of the Pareto front or the area covered by the Pareto front with respect to a point selected in the dominated region [54,55].

The natures of the solutions are illustrated in Fig. 6. These results are also supported by the time domain evolution of the states of the chaotic system under the action of different controllers in Fig. 7. The interpretations of the results are similar for the commensurate case. Fig. 7 shows that state y settles fastest to the equilibrium point in solution A_2 followed by solutions B_2 and C_2, whereas solution C_2 exhibits the slowest response. However, the control effort required for state y is the least with solution C_2 and the highest with solution A_2, while that for B_2 is between these two cases.

For the incommensurate FO system, each of the three FOs of the three state variables are decreased gradually one at a time from their nominal values that exhibit chaos, i.e., $q_1 = 0.9$, $q_2 = 0.95$, $q_3 = 0.8$, while maintaining the other two FOs as constant. In a scenario where the incommensurate orders are changed separately, the chaos disappears below $q_1 < 0.8$, $q_2 < 0.85$, $q_3 < 0.5$. However, for all the changes in the system order, the same active control policy is capable of suppressing the chaotic oscillations in both the commensurate and incommensurate FO financial systems, as shown by the phase portraits of the systems under active control in Figs. 5 and 8, respectively. In the present study, with the same controller, the system satisfies the analytical stability condition given by Matignon's theorem. As expected, the common control policy for the perturbed system will not be Pareto optimal compared with different controllers that are tuned for specific fixed values of the commensurate and incommensurate orders. However, these solutions are still good results in terms of chaos suppression.

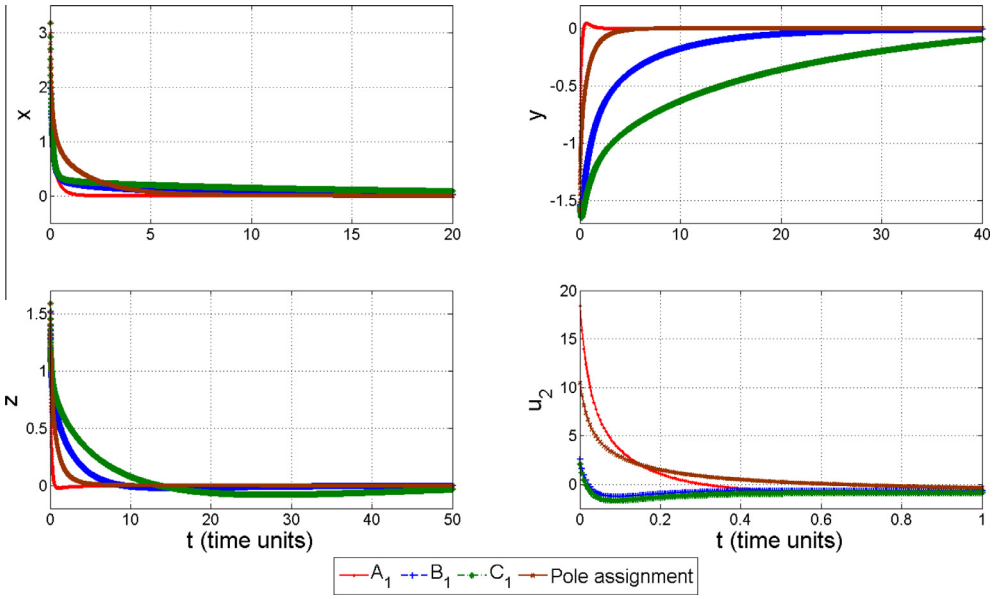

Fig. 4. Chaos control with representative solutions on the Pareto front for the commensurate FO financial system.

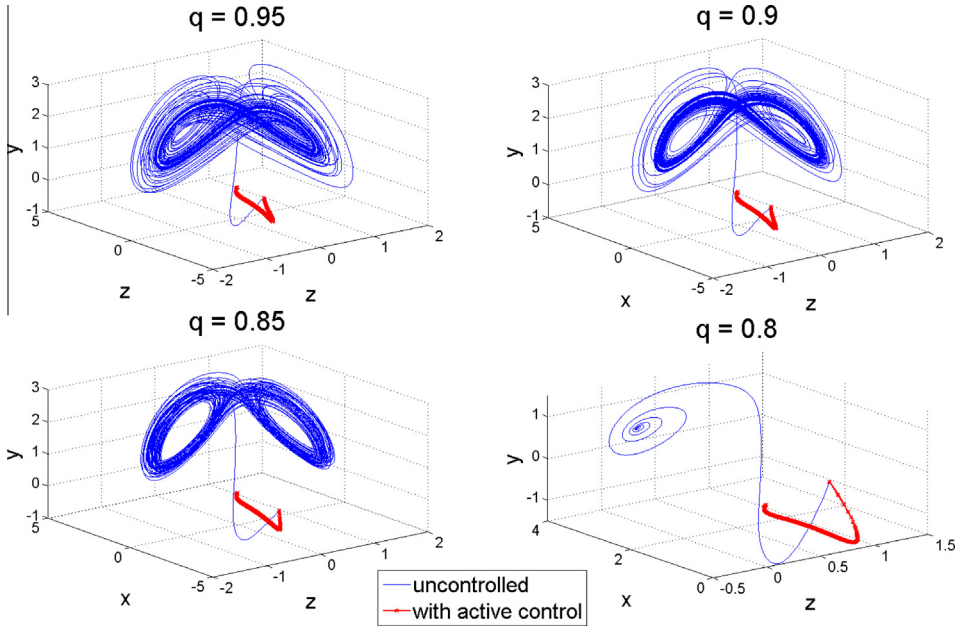

Fig. 5. Uncontrolled and active controlled phase portraits of the changes in the commensurate FO financial system with the median solution (B_1) on the Pareto front.

5.3. Comparison with direct pole assignment-based active control approach

Most other controller design methods for FO chaotic systems select the active control functions heuristically so the eigenvalues are obtained in the stable region. Bhalekar and Gejji [41] showed that an active control scheme can be designed intuitively so all of the eigenvalues in the stability matrix become (-1) for a commensurate FO chaotic system. After a similar treatment of the commensurate order system, the P matrix in (17) needs to be diagonalized such that the diagonal elements

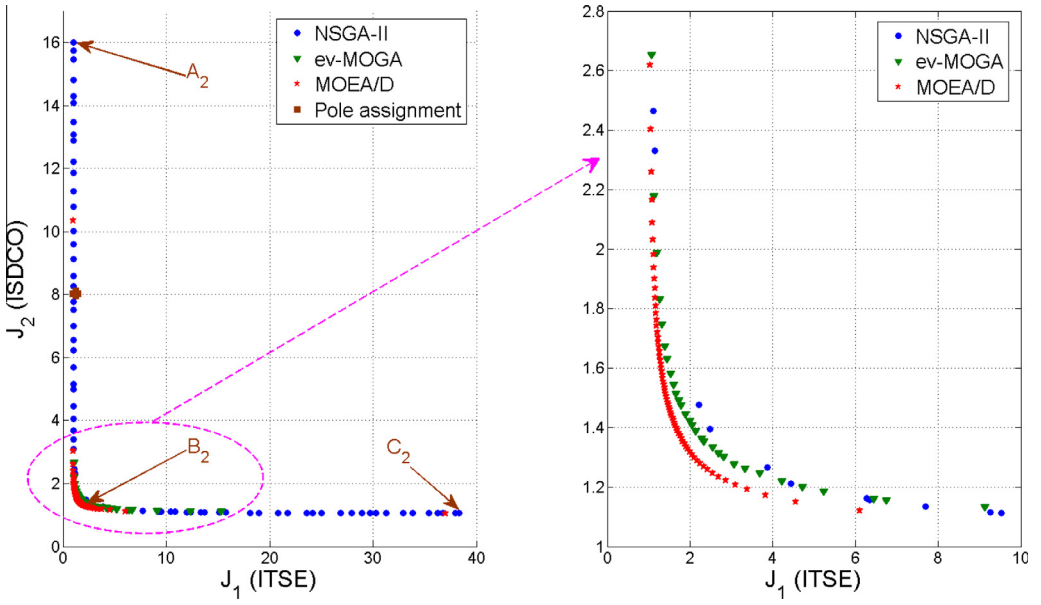

Fig. 6. Pareto optimal front for the incommensurate FO financial system.

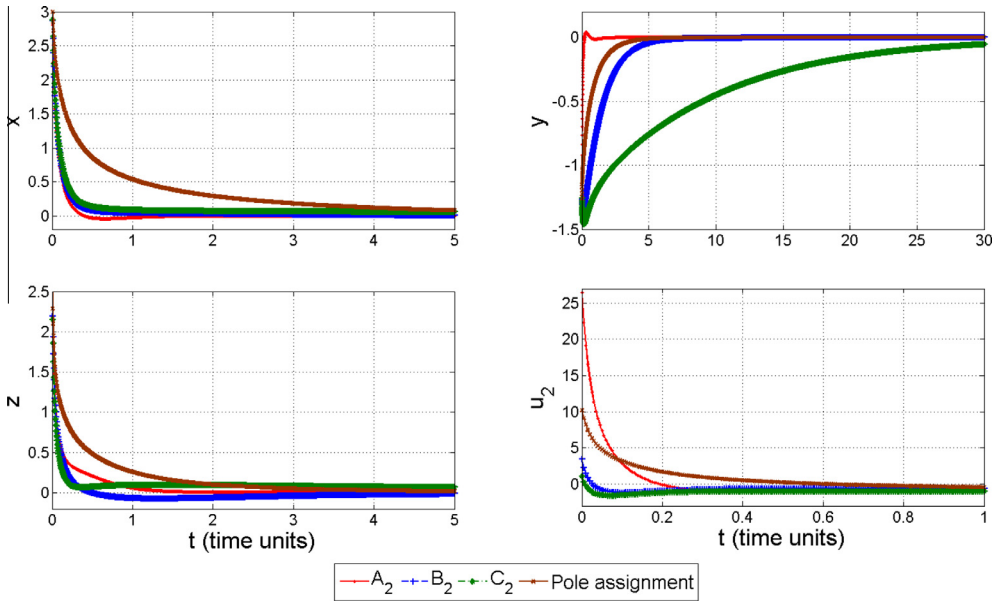

Fig. 7. Chaos control with representative solutions on the Pareto front for the incommensurate FO financial system.

are the desired eigenvalues. The corresponding choice of constants m_{ij} in (16) becomes $[m_{ij}] = \begin{bmatrix} a+\bar{a} & 0 & -1 \\ 0 & b+\bar{b} & 0 \\ 1 & 0 & c+\bar{c} \end{bmatrix}$ to make the matrix $P = \begin{bmatrix} \bar{a} & 0 & 0 \\ 0 & \bar{b} & 0 \\ 0 & 0 & \bar{c} \end{bmatrix}$.

In this case, the desired roots of the chaotic system under active control are set as $\bar{a} = \bar{b} = \bar{c} = -1$. This framework is applied to both the commensurate and incommensurate FO systems under study.

As expected, an intuitive choice will never produce the optimum results obtained using the proposed MOO framework. To highlight this point, Fig. 3 shows the performance of the controlled system in the two-dimensional space between two conflicting objectives using the active control design method proposed by Bhalekar and Gejji [41] for commensurate FO chaotic

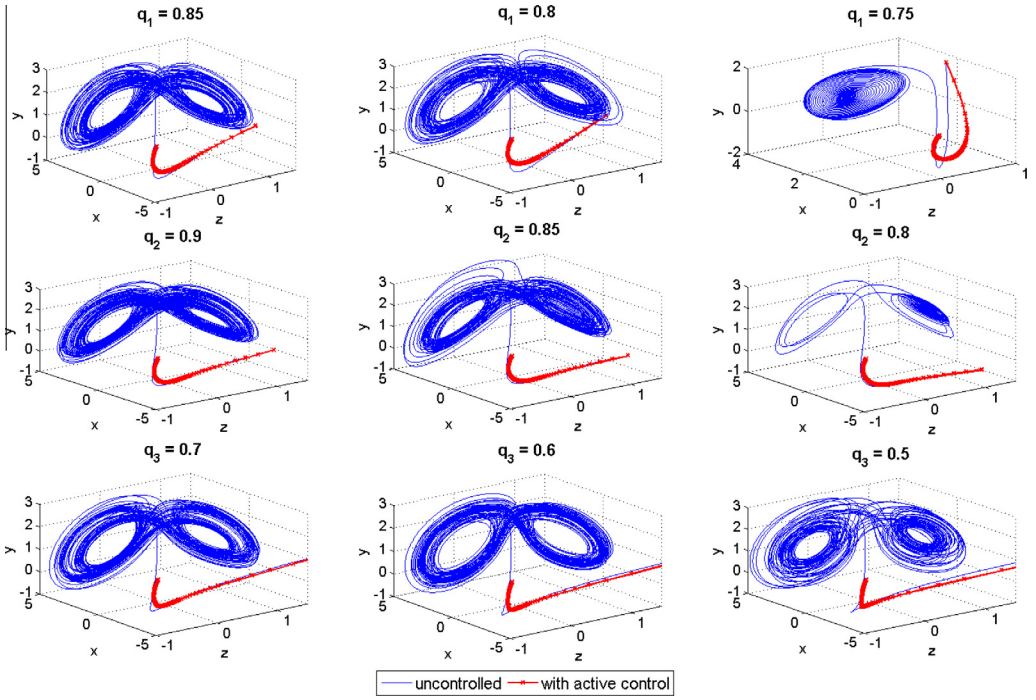

Fig. 8. Uncontrolled and active controlled phase portraits based on gradual decreases in the incommensurate FO financial system orders from their nominal values $q_1 = 0.9$, $q_2 = 0.95$, $q_3 = 0.8$, with the median solution (B_2) on the Pareto front.

systems. This approach cannot be extended easily to incommensurate order systems because only the stable roots within the primary Riemann sheet are normally considered in these systems. In addition, depending on the incommensurate FOs and the least common multiple (LCM) of the associated denominators of these fractions q_i, there may be a variable number of roots and it is difficult to assign them using an approach similar to that proposed for the commensurate order case by Bhalekar and Gejji [41].

In this case, the LCM of q_i is $m = 20$ for the incommensurate orders selected for the system, i.e., $q_1 = 0.9$, $q_2 = 0.95$, $q_3 = 0.8$. To obtain the characteristic equation in the form of the desired roots, the choice of the constants in (16) are $m_{11} = a + \bar{a}$, $m_{22} = b + \bar{b}$, $m_{33} = c + \bar{c}$, $m_{12} = m_{21} = m_{23} = m_{32} = 0$, $m_{13} = -1$, and $m_{31} = 1$ in order to produce the stability matrix $P = \begin{bmatrix} -a + m_{11} & m_{12} & 1 + m_{13} \\ m_{21} & -b + m_{22} & m_{23} \\ -1 + m_{31} & m_{32} & -c + m_{33} \end{bmatrix} = \begin{bmatrix} -1 & 0 & 0 \\ 0 & -1 & 0 \\ 0 & 0 & -1 \end{bmatrix}$.

Using this selection, the desired pole locations are $\bar{a} = \bar{b} = \bar{c} = -1$ and the characteristic equation becomes (23).

$$det[s^{q_i} I - P] = \det\left[(diag[\lambda^{mq_1} \quad \lambda^{mq_2} \quad \lambda^{mq_3}]) - P\right] = \begin{bmatrix} \lambda^{18} + 1 & 0 & 0 \\ 0 & \lambda^{19} + 1 & 0 \\ 0 & 0 & \lambda^{16} + 1 \end{bmatrix}. \tag{23}$$

As a result, the characteristic equation (23) yields several roots λ_i, which satisfy the incommensurate version of Matignon's stability criterion. For the current direct pole assignment scheme for the incommensurate FO system, all the roots of the characteristic equation lie in the hyper-damped region, i.e., $|\arg(\lambda_i)| > q\pi$, which indicates the stable but slower operation of the system compared with that achieved within a MOO framework. The dominated solution is obtained using the direct pole assignment technique rather than the Pareto solutions (in terms of control performance) because the pole assignment scheme obtains all hyper-damped and ultra-damped roots [33], thereby leading to slow system operation and an increase in the control effort required. Unlike the commensurate FO system, precise pole assignment becomes difficult in the incommensurate FO system stabilization problem due to the inherent higher order polynomial equation solution step. We can assign the eigenvalues of the matrix P analytically, but manipulating the numbers and locations of all the system roots of the characteristic equation that are distributed in different higher Riemann sheets for any arbitrary choice of incommensurate FO is still an open problem. Moreover, only one solution is obtained by the direct pole-assignment approach for the commensurate order system, whereas multiple solutions are generated for the incommensurate FO system. As shown in Fig. 6, the direct pole assignment approach also leads to a dominated solution for the incommensurate system compared with that obtained using a MOO approach.

5.4. Discussion

It is important to mention that FO controllers have been traditionally used to enhance the robust stability properties of linear control systems. For nonlinear chaotic systems, however, extensions of the robust stability properties are expected to be more complex and they have not yet been investigated by the fractional calculus community, to the best of our knowledge. Moreover, the proposed control strategy does not use the FO controller concept, but instead it employs the nonlinear state feedback control of FO systems. For both the commensurate and incommensurate order systems, the active control scheme designed using the nominal system parameters faithfully suppresses chaotic oscillations with gradual decreases in FOs and it also satisfies the stability checking condition, but this variation has not been considered during the controller design phase. Therefore, the same controller works well in stabilizing different FO chaotic systems, but this should not be confused with robust stability where the stability of all possible intermediate solutions are theoretically guaranteed, which has only been investigated for linear FO systems in previous studies.

6. Conclusions

In this study, an active control policy is proposed for a FO chaotic financial system. The proposed method gives guaranteed stability, which is derived analytically for both commensurate and incommensurate FO financial systems. The active control functions are selected using three multi-objective evolutionary algorithms to satisfy two conflicting time domain performance objectives, i.e., rapid settling to the equilibrium point and a requirement for low controller effort. Our comparison of three MOOs showed that the NSGA-II yields the largest Pareto front compared with εv-MOGA and MOEA/D, but a better non-dominated (although shorter) Pareto front could be achieved using MOEA/D. We showed that the two design objectives cannot be minimized simultaneously using one particular controller. A range of controllers on the Pareto front satisfy one criterion better but at the cost of performance degradation in terms of other criterion. Thus, the designer can select a particular controller from the set of non-dominated solutions according to their specific problem requirements. We also demonstrated the superiority of the proposed technique compared with the direct pole assignment approach [41]. Decreasing the FOs in the two types of systems (with the median solution of the controllers on the Pareto front) was shown to stabilize the chaotic systems and they also satisfied the stability checking conditions. Future work should focus on multi-objective chaos control in the presence of uncertainty, noise, etc., and extend the concept to robust stabilization scheme designs for nonlinear chaotic systems.

References

[1] T. Puu, Attractors, Bifurcations, & Chaos: Nonlinear Phenomena in Economics, Springer, 2003.
[2] S. Rostek, Option Pricing in Fractional Brownian Markets, vol. 622, Springer, 2009.
[3] J. Tenreiro Machado, F.B. Duarte, G.M. Duarte, Power law analysis of financial index dynamics, Discrete Dyn. Nat. Soc. 2012 (2012), http://dx.doi.org/10.1155/2012/120518. Article ID 120518, 12 pages.
[4] F.B. Duarte, J. Tenreiro Machado, G. Monteiro Duarte, Dynamics of the Dow Jones and the NASDAQ stock indexes, Nonlinear Dyn. 61 (4) (2010) 691–705.
[5] M.M. Meerschaert, E. Scalas, Coupled continuous time random walks in finance, Phys. A 370 (1) (2006) 114–118.
[6] J.T. Machado, G.M. Duarte, F.B. Duarte, Identifying economic periods and crisis with the multidimensional scaling, Nonlinear Dyn. 63 (4) (2011) 611–622.
[7] M.-F. Danca, R. Garrappa, W.K. Tang, G. Chen, Sustaining stable dynamics of a fractional-order chaotic financial system by parameter switching, Comput. Math. Appl. 66 (5) (2013) 702–716.
[8] R.V. Mendes, A fractional calculus interpretation of the fractional volatility model, Nonlinear Dyn. 55 (4) (2009) 395–399.
[9] Y. Xu, Z. He, Synchronization of variable-order fractional financial system via active control method, Cent. Eur. J. Phys. 11 (6) (2013) 824–835.
[10] T. Skovránek, I. Podlubny, I. Petrás, Modeling of the national economies in state-space: a fractional calculus approach, Econ. Model. 29 (4) (2012) 1322–1327.
[11] Z. Hu, W. Chen, Modeling of macroeconomics by a novel discrete nonlinear fractional dynamical system, Discrete Dyn. Nat. Soc. 2013 (2013), http://dx.doi.org/10.1155/2013/275134. Article ID 275134, 9 pages.
[12] Y. Yue, L. He, G. Liu, Modeling and application of a new nonlinear fractional financial model, J. Appl. Math. 2013 (2013), http://dx.doi.org/10.1155/2013/325050. Article ID 325050, 9 pages.
[13] Z. Wang, X. Huang, G. Shi, Analysis of nonlinear dynamics and chaos in a fractional order financial system with time delay, Comput. Math. Appl. 62 (3) (2011) 1531–1539.
[14] Q. Gao, J. Ma, Chaos and Hopf bifurcation of a finance system, Nonlinear Dyn. 58 (1–2) (2009) 209–216.
[15] H. Yu, G. Cai, Y. Li, Dynamic analysis and control of a new hyperchaotic finance system, Nonlinear Dyn. 67 (3) (2012) 2171–2182.
[16] D. Guegan, Chaos in economics and finance, Annu. Rev. Control 33 (1) (2009) 89–93.
[17] J. Holyst, M. Zebrowska, K. Urbanowicz, Observations of deterministic chaos in financial time series by recurrence plots, can one control chaotic economy?, Eur Phys. J. B 20 (4) (2001) 531–535.
[18] W.A. Brock, C.H. Hommes, Heterogeneous beliefs and routes to chaos in a simple asset pricing model, J. Econ. Dyn. Cont. 22 (8–9) (1998) 1235–1274.
[19] J.M. González-Miranda, Synchronization and Control of Chaos: An Introduction for Scientists and Engineers, Imperial College Press, 2004.
[20] H. Zhang, D. Liu, Z. Wang, Controlling Chaos: Suppression, Synchronization and Chaotification, Springer, 2009.
[21] W.-C. Chen, Nonlinear dynamics and chaos in a fractional-order financial system, Chaos, Solitons Fractals 36 (5) (2008) 1305–1314.
[22] S. Dadras, H.R. Momeni, Control of a fractional-order economical system via sliding mode, Phys. A 389 (12) (2010) 2434–2442.
[23] W.-C. Chen, Dynamics and control of a financial system with time-delayed feedbacks, Chaos, Solitons Fractals 37 (4) (2008) 1198–1207.
[24] L. Chen, Y. Chai, R. Wu, Control and synchronization of fractional-order financial system based on linear control, Discrete Dyn. Nat. Soc. 2011 (2011).
[25] G. Cai, P. Hu, Y. Li, Modified function lag projective synchronization of a financial hyperchaotic system, Nonlinear Dyn. 69 (3) (2012) 1457–1464.
[26] M.S. Abd-Elouahab, N.-E. Hamri, J. Wang, Chaos control of a fractional-order financial system, Math. Prob. Eng. 2010 (2010), http://dx.doi.org/10.1155/2010/270646. Article ID 270646, 18 pages.
[27] Z. Wang, X. Huang, H. Shen, Control of an uncertain fractional order economic system via adaptive sliding mode, Neurocomputing 83 (2012) 83–88.

[28] W.-D. Chang, PID control for chaotic synchronization using particle swarm optimization, Chaos, Solitons Fractals 39 (2) (2009) 910–917.
[29] I. Pan, A. Korre, S. Das, S. Durucan, Chaos suppression in a fractional order financial system using intelligent regrouping PSO based fractional fuzzy control policy in the presence of fractional Gaussian noise, Nonlinear Dyn. 70 (4) (2012) 2445–2461.
[30] S. Das, I. Pan, S. Das, A. Gupta, Master–slave chaos synchronization via optimal fractional order PIλDμ controller with bacterial foraging algorithm, Nonlinear Dyn. 69 (4) (2012) 2193–2206.
[31] Y. Tang, Z. Wang, W. Wong, J. Kurths, J. Fang, Multiobjective synchronization of coupled systems, Chaos: An Interdiscipl. J. Nonlinear Sci. 21 (2) (2011) 025114.
[32] I. Petras, Fractional-order Nonlinear Systems: Modeling, Analysis and Simulation, Springer, 2011.
[33] S. Das, Functional Fractional Calculus, Springer, 2011.
[34] K. Diethelm, N.J. Ford, A.D. Freed, A predictor–corrector approach for the numerical solution of fractional differential equations, Nonlinear Dyn. 29 (1–4) (2002) 3–22.
[35] Y.Q. Chen, I. Petras, D. Xue, Fractional order control – a tutorial, in: American Control Conference 2009, ACC'09, 2009, pp. 1397–1411.
[36] A. Oustaloup, F. Levron, B. Mathieu, F.M. Nanot, Frequency-band complex noninteger differentiator: characterization and synthesis, IEEE Trans. Circuits Syst. I: Fundam. Theory Appl. 47 (1) (2000) 25–39.
[37] Y. Chen, Oustaloup-recursive-approximation for fractional order differentiators, 2003. [Online]. Available from: <http://www.mathworks.co.uk/matlabcentral/fileexchange/3802-oustaloup-recursive-approximation-for-fractional-order-differentiators>.
[38] D. Matignon, Stability properties for generalized fractional differential systems, in: ESAIM Proceedings, vol. 5, 1998, pp. 145–158.
[39] W. Deng, C. Li, J. Lü, Stability analysis of linear fractional differential system with multiple time delays, Nonlinear Dyn. 48 (4) (2007) 409–416.
[40] M.S. Tavazoei, M. Haeri, Chaotic attractors in incommensurate fractional order systems, Physica D 237 (20) (2008) 2628–2637.
[41] S. Bhalekar, V. Daftardar-Gejji, Synchronization of different fractional order chaotic systems using active control, Commun. Nonlinear Sci. Numer. Simul. 15 (11) (2010) 3536–3546.
[42] S. Das, S. Mukherjee, S. Das, I. Pan, A. Gupta, Continuous order identification of PHWR models under step-back for the design of hyper-damped power tracking controller with enhanced reactor safety, Nucl. Eng. Des. 257 (2013) 109–127.
[43] H.M. Hochman, J.D. Rodgers, Pareto optimal redistribution, Am. Econ. Rev. (1969) 542–557.
[44] A. Herreros, E. Baeyens, J.R. Perán, Design of PID-type controllers using multiobjective genetic algorithms, ISA Trans. 41 (4) (2002) 457–472.
[45] I. Pan, S. Das, Chaotic multi-objective optimization based design of fractional order PIλDμ controller in AVR system, Int. J. Electr. Power Energy Syst. 43 (1) (2012) 393–407.
[46] G. Reynoso-Meza, S. Garcia-Nieto, J. Sanchis, F.X. Blasco, Controller tuning by means of multi-objective optimization algorithms: a global tuning framework, IEEE Trans. Control Syst. Technol. 21 (2) (2013) 445–458.
[47] K. Deb, A. Pratap, S. Agarwal, T. Meyarivan, A fast and elitist multiobjective genetic algorithm: NSGA-II, IEEE Trans. Evol. Comput. 6 (2) (2002) 182–197.
[48] M.T. Jensen, Reducing the run-time complexity of multiobjective EAs: the NSGA-II and other algorithms, IEEE Trans. Evol. Comput. 7 (5) (2003) 503–515.
[49] M. Laumanns, L. Thiele, K. Deb, E. Zitzler, Combining convergence and diversity in evolutionary multiobjective optimization, Evol. Comput. 10 (3) (2002) 263–282.
[50] K. Deb, M. Mohan, S. Mishra, Evaluating the ε-domination based multi-objective evolutionary algorithm for a quick computation of Pareto-optimal solutions, Evol. Comput. 13 (4) (2005) 501–525.
[51] M. Martinez-Iranzo, J.M. Herrero, J. Sanchis, X. Blasco, S. Garcia-Nieto, Applied Pareto multi-objective optimization by stochastic solvers, Eng. Appl. Artif. Intell. 22 (3) (2009) 455–465.
[52] J. Herrero, M. Martinez, J. Sanchis, X. Blasco, Well-distributed Pareto front by using the ε-MOGA evolutionary algorithm, in: Computational and Ambient Intelligence, Springer, 2007, pp. 292–299.
[53] Q. Zhang, H. Li, MOEA/D: a multiobjective evolutionary algorithm based on decomposition, IEEE Trans. Evol. Comput. 11 (6) (2007) 712–731.
[54] E. Zitzler, L. Thiele, Multiobjective optimization using evolutionary algorithms—a comparative case study, in: Parallel Problem Solving from Nature—PPSN V, 1998, pp. 292–301.
[55] E. Zitzler, L. Thiele, Multiobjective evolutionary algorithms: a comparative case study and the strength Pareto approach, IEEE Trans. Evol. Comput. 3 (4) (1999) 257–271.